Performance Analysis of Model Predictive Controllers for Active Cell Balancing of Electric Vehicle Battery

Afaq Ahmed[1], Ali Arshad Uppal[1], Qadeer Ahmed[2] and [1]Muhammad Rizwan Azam

***Abstract*— One of the functionalities of a battery management system (BMS) in an Electric Vehicle (EV) is to ensure that charge among cells is equally distributed, potentially leading to enhanced performance and reliability. In this context, Model Predictive Control (MPC) has emerged as a suitable candidate. In this work, a battery pack consisting of two serially connected cells along with the bi-directional buck-boost converter is employed to simulate the balancing phenomena. Moreover, to calculate the mean balancing currents and power losses of active cell balancing architecture (ACBN) , a high-fidelity model is considered. The purpose is to rigorously investigate the impact of selecting different cost functions in MPC formulation on the closed-loop performance of ACBN in terms of balancing time t_b and average power losses $\bar{P}_L$. To this end, a non-linear model predictive control (NMPC) is formulated to perform active balancing, and the problem is subsequently solved in CasADi framework employing interior point optimizer (Ipopt) algorithm. To mimic the realistic conditions, a US06 City current profile is taken as in input and the simulation's results demonstrates a noteworthy 38.9 $\%$ disparity in t_b and a 4.5 $\%$ difference in $\bar{P}_L$ across distinct cost functions, underscoring the need for selecting the optimal cost function within the active cell balancing domain.**

I. Introduction

In the domain of electric vehicles, a battery management system (BMS) plays a critical role. A BMS is equipped with functionalities that constitute the estimation and regulation of important batteries's parameters, i.e., current, voltages, state of charge (SoC), temperature, etc. By doing so, the BMS ensures the maximum utilization of the battery's capabilities in an optimal manner. One of the tasks of BMS is to make sure that charge is evenly distributed among cells. This is important because if any cell in a serially connected topology fully discharges, then the full battery pack is shut down. To this end, a BMS resorts to charge balancing via two main approaches: passive and active cell balancing (ACB). The key distinction between these approaches lies in their handling of charges: the passive technique expends the excess charge/energy via a resistor, whereas the ACB conserves the charge by allocating it to charge-deprived cells.

In the context of ACB, controllers are usually employed to maintain uniform charge distribution. In this vein, model predictive control (MPC) has garnered attention due to its inherent capabilities for handling non-linear coupled systems and actuator and state constraints. For instance, in [1], the authors employed the NMPC framework to achieve the task of charge balancing between two cells while simultaneously keeping the energy expenditure to a minimum. Moreover, within the scope of MPC based equalization, [2] also addressed the issue of associated computational cost by keeping the prediction horizon at a lower value. To achieve that, they included multiple terms related to charge, SoC, and voltages in the cost function. Also focusing on the impact of changing terms in the cost function of MPC, [3] investigated its three variations and its subsequent impact on balancing and EV's range. Similarly, in [4], the authors focused on minimizing the balancing currents as well as keeping the SoC of all cells to the average value. To achieve that, they formulated an optimization problem employing the Cuk converter and solved it via quadratic programming. Building upon that, [5] increased the model's scope by appending a thermal model to it for the balancing problem. [6] used the soft actor critic (SAC) algorithm for fast charging, cell balancing, and temperature regulation for Li-ion batteries. Moreover, they also provided a comparative analysis of SAC and MPC. By exploiting the differential flatness property of ACBN, [7] set up a multi-objective optimal control problem with the aim of minimizing power losses and balancing time. [8], developed a convex optimization problem to balance the SoC, while concurrently addressing thermal and voltage equalization. Further research delves into various balancing topologies and control algorithms to achieve objectives like temperature control and reduced charging durations [9]–[11], with other research also focusing on the upsides of ACB, such as battery repurposing and decelerating aging phenomena, etc [12], [13]. Similarly, researchers have also incorporated physics-based battery models in optimal control of ACB paradigm. For instance, [14] have utilized single particle model (SPM) that also models the electrolyte and temperature dynamics in the NMPC formulation to tackle various conflicting sub-objectives. [15] used an SPM model that incorporates aging and thermal dynamics to design and solve a nonlinear optimal control problem aimed at achieving fast charging with minimal degradation of a lithium-ion battery (LiB).

In our prior study [16], a power losses-aware NMPC for ACB network (ACBN) was developed, yet that analysis overlooked the impact of the selection of various cost functions, and their subsequent impact on the closed-loop performance, particularly in terms of power losses $\bar{P}_L$ and balancing time t_b. This work aims to bridge this gap by incorporating three distinct cost functions into NMPC formulation and provide a comparative performance analysis of ACBN.

The rest of the paper is organized as follows. The battery

[1]Afaq Ahmed, [1]A. A. Uppal and [1]M. Rizwan Azam are with the Department of Electrical and Computer Engineering, COMSATS University Islamabad, Islamabad 44000, Pakistan.

[2]Qadeer Ahmed is with the Center for Automotive Research, The Ohio State University, Columbus, OH 43210 USA.

model along with ACBN is given in section II. Section III formulates the NMPC problem for ACB. Section IV presents the results and discussion; and the paper is concluded in section V.

II. Mathematical Modeling of the Cell Balancing Network

To perform the active cell balancing of two serially connected cell, a bidirectional buck-boost converter, which operates in discontinuous current mode, is employed. Similarly, how an EV communicates with ACB via the cascades of submodules, I.e electric motor, inverter, is illustrated in Figure 2. The working mechanism of the ACBN is as follows: when cell-1 has a higher SoC, it transfers its excess charge to inductor L upon the activation of MOSFET Q1. The inductor L, acting as an intermediary storage device, then charges the other cell via diode Q_2. Conversely, cell-2 charges cell-1 through the intermediary devices Q_2 and D_1. Moreover, due to physical constraints, Q_1 and Q_2 can't be activated at the same instant. The mathematical model is adopted from our previous work [16] and is given in the following sub-sections.

A. Mean Balancing Currents in ACBN

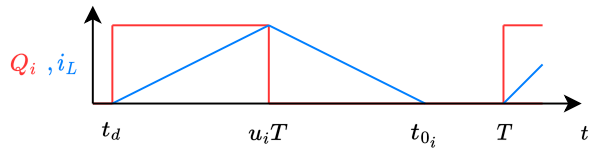

Fig. 1: Switching cycle of Q_i and mean balancing current.

The switching period of Q_i and the corresponding inductor current i_L is shown in Figure 1, which is expressed as

$$i_L = \begin{cases} 0, & 0 \le t \le t_d \\ \dfrac{v_H}{R_{ch_i}}\Big(1-\exp(\lambda_i)\Big), & t_d \le t \le u_iT \\ \exp(\phi_i)\Big(I_{P_i}+\dfrac{v_L+V_F}{R_{dis_i}}\Big)-\dfrac{v_L+V_F}{R_{dis_i}}, & u_iT \le t \le t_{0_i} \\ 0, & t_{0_i} \le t \le T \end{cases}, \tag{1}$$

$$\lambda_i = \frac{t_d - t}{\tau_{ch_i}},\ \phi_i = \frac{u_iT - t}{\tau_{dis_i}},\ R_{dis_i} = R_{0_L} + R_L,$$
$$R_{ch_i} = R_{0_H} + R_L + R_{ds},\ \tau_{ch_i} = L/R_{ch_i},\ \tau_{dis_i} = L/R_{dis_i},$$

where $i = 1$ and $i = 2$ denote the cases where cell-1 charges cell-2 and cell-2 charges cell-1, respectively. The symbols v_H, v_L and R_{0_H}, R_{0_L} represent the open circuit voltages (V) and resistances (Ω) of the cells with higher and lower SoC, respectively. The diode forward voltage drop is represented by V_F. The time constants (s) for the charging and discharging paths are denoted by τ_{ch} and τ_{dis} , respectively. The symbols t_d, t_0, and T stand for the dead time, the time instant when $i_L = 0$, and the switching time period, respectively. The duty cycle of Q_i is indicated by u_i, and L represents the inductance of the inductor (H). The resistances of the charging path, discharging path, cell i, inductor, and on-state switching are represented by R_{ch}, R_{dis}, R_L, and R_{ds}, respectively.

When cell-1 transfers charge to cell-2, u_i becomes equal to u_1, v_H to v_1, and v_L to v_2; in the other way around, u_i becomes equal to u_2, v_H to v_2, and v_L to v_1.

Moreover, to obtain the mean currents of an inductor for both charging and discharging mode, equation (1) is integrated over the whole switching period.

$$\tilde{I}_{ch_i} = \frac{v_H}{TR_{ch_i}}\Big(u_iT - t_d + \tau_{ch_i}(\exp(\kappa_i)-1)\Big), \tag{2}$$

$$\tilde{I}_{dis_i} = \frac{\tau_{dis_i}(\exp(\chi_i)-1)}{T}\left(-I_{P_i} - \frac{a_{0_i}(t_{0_i}-u_iT)}{\tau_{dis_i}(\exp(\chi_i)-1)} + 1\right), \tag{3}$$

$$I_{P_i} = \frac{v_H}{R_{ch_i}}\Big(1-\exp(\kappa_i)\Big),\ \kappa_i = \frac{t_d - u_iT}{\tau_{ch_i}},$$
$$t_{0_i} = u_iT + \tau_{dis_i} ln\left(\frac{R_{dis_i}v_H}{(v_L+V_F)R_{ch_i}}(1-\exp(\kappa_i))+1\right),$$
$$\chi_i = \frac{u_iT - t_{0_i}}{\tau_{dis_i}},\ a_{0_i} = \frac{v_L+V_F}{R_{dis_i}},$$

where $\tilde{I}_{ch}$ and $\tilde{I}_{dis}$ represents the mean currents (A) of inductor during charging and discharging modes respectively; I_p is the peak inductor current at $t = u_iT$ (cf. figure 1)

B. Power Losses in the Buck-Boost Converter

Multiple factors partake in determining the conduction losses: cells's internal resistance, diode resistance in on-state, energy storage elements' parasitic resistance, and MOSFETs' power losses. They are defined as follows:

$$P_{con} = \sum_{j=1}^{2}\left[\tilde{I}_{ch_j}^2\tilde{R}_{ch}u_j + \tilde{I}_{dis_j}^2\tilde{R}_{dis}\left(\frac{t_{0_j}-u_jT}{T}\right)\right] + \sum_{j=1}^{2} I_{b_j}^2 R_{0_j}, \tag{4}$$

$$\tilde{I}_{ch_j}^2 = \frac{v_h^2}{TR_{ch}^2}\left[\tau_{ch}e^{\kappa_j}\left(\frac{4-e^{\kappa_j}}{2}\right) + u_jT - t_d - \frac{3}{2}\tau_{ch}\right]$$

$$\tilde{I}_{dis_j}^2 = \frac{1}{T}\left[\tau_{dis}I_{p_j}\left(\frac{I_{p_j}}{2} - a_0\right) + a_0^2\left(t_0 - u_jT - \frac{3}{2}\tau_{dis}\right)\right] + \frac{1}{T}\left[-\tau_{dis}e^{2\kappa_j}\left(\frac{I_{p_j}^2}{2} + \frac{a_0^2}{2} + a_0I_{p_j}\right)\right] + \frac{1}{T}\left[e^{3\kappa_j}2a_0\tau_{dis}\left(I_{p_j}+a_0\right)\right],$$

where P_{con} represents conduction losses (W); $\tilde{R}_{ch} = R_{ch} - R_{0_h}$, $\tilde{R}_{dis} = R_{dis} - R_{0_l}$; I_{b_j}, cf. (10), (11), is the current of cell-j; and $\tilde{I}_{ch}$ and $\tilde{I}_{dis}$ represent the RMS currents during charging and discharging modes, respectively.

Since the buck-boost converter operates in discontinuous conduction mode, the switching losses account only for the power losses when the MOSFETs are off

$$P_{t_f} = \frac{t_f}{2T}\sum_{j=1}^{2} v_h I_{dis_j}, \tag{5}$$

where t_f is the fall time.

The body diodes' reverse recovery power loss is as follows

$$P_{D_{rr}} = \frac{t_{rr}^2}{2TL} \sum_{j=1}^{2} v_j v_F, \tag{6}$$

where $P_{D_{rr}}$ and t_{rr} represent the reverse recovery power loss, and time, respectively.

The inductor discharges through the body diodes while in dead time since Q_1 and Q_2 are off. Thus, the dead time power losses are given as

$$P_{t_d} = \frac{V_F t_d}{2T} \sum_{j=1}^{2} I_{dis_j}, \tag{7}$$

where P_{t_d} and t_d represents dead time power loss and dead time respectively.

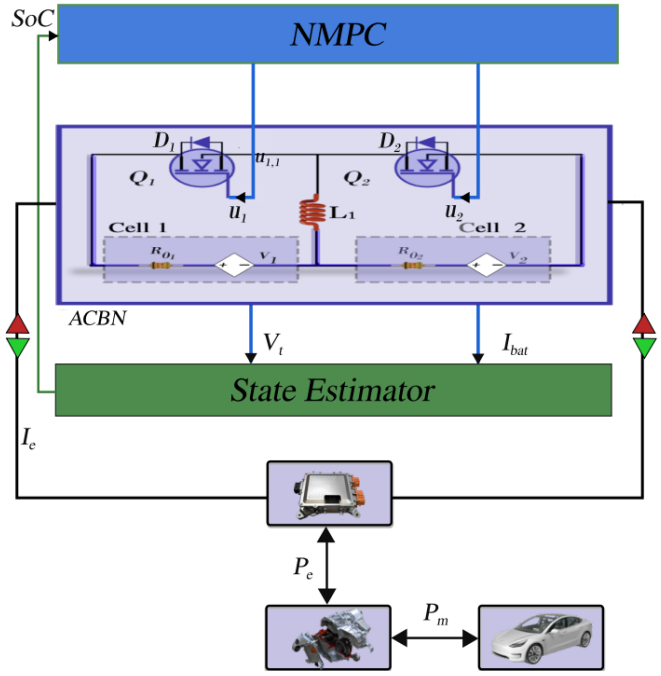

Fig. 2: Interaction of EV with ACBN.

C. Equivalent Circuit Model of the Battery Pack

Since physics-based models aren't computationally feasible, an ECM-based model is considered, which includes cells's internal resistance R_{0_i} connected in series with a dependent voltage source v_i— open circuit voltage. The battery pack model is given as

$$\dot{\mathbf{x}} = \mathbf{f}(\mathbf{x}, \mathbf{u}) = \begin{bmatrix} \frac{I_{b_1}}{\eta_1} & \frac{I_{b_2}}{\eta_2} \end{bmatrix}^T, \tag{8}$$

$$\mathbf{v}_t = \mathbf{h}(\mathbf{x}, \mathbf{u}) = \begin{bmatrix} v_1 + I_{b_1} R_{0_1} & v_2 + I_{b_2} R_{0_2} \end{bmatrix}^T, \tag{9}$$

$$I_{b_1} = -\tilde{I}_{ch_1}(u_1, x_1) + \tilde{I}_{dis_2}(u_2, x_1, x_2) + I_e(t), \tag{10}$$

$$I_{b_2} = -\tilde{I}_{ch_2}(u_2, x_2) + \tilde{I}_{dis_1}(u_1, x_1, x_2) + I_e(t), \tag{11}$$

$$v_i = \sum_{j=1}^{8} p_j x_i^{(8-j)}, \tag{12}$$

where $\mathbf{x} \in \Re^2$ is the state vector denoting the SoC of cell-1 (x_1) and cell-2 (x_2), respectively; $\mathbf{u} \in \Re^2$ is the control vector representing the duty cycles of Q_1 and Q_2, respectively; $\mathbf{v}_t \in \Re^2$ denotes the terminal voltages of the cells; η_i is the capacity of cell-i (in ampere-seconds, As); and $p = [88.56, : -320.46, : 472.36, : -368.96, : 166.57, : -44.01, : 7.18, : 2.95]$.

III. NMPC Design for ACBN

In this section three NMPC are designed to solve the following nonlinear optimal control problem (NOCP)

$$\min_{\mathbf{x}(k), \mathbf{d}(k)} J_i(\mathbf{x}(k), \mathbf{d}(k)),$$

subject to:

$$\begin{aligned}
&\mathbf{x}(k+1) - \mathbf{f}(\mathbf{x}(k), \mathbf{d}(k)) = 0,\\
&\mathbf{x}(k_0) = \mathbf{x}_{k_0},\\
&\tilde{d}_1(k)\tilde{d}_2(k) = 0,\\
&\underline{\mathbf{d}} \le \mathbf{d}(k) \le \bar{\mathbf{d}},\\
&\underline{\mathbf{x}} \le \mathbf{x}(k) \le \bar{\mathbf{x}},\\
&\underline{\mathbf{d}}^T = [0.1 \;\; 0.1],\\
&\bar{\mathbf{d}}^T = [0.4 \;\; 0.4],\\
&\underline{\mathbf{x}}^T = [0.05 \;\; 0.05],\\
&\bar{\mathbf{x}}^T = [0.95 \;\; 0.95]
\end{aligned}$$

where J_i, for $i = \{1, 2, 3\}$, represents the cost function to be minimized; $\mathbf{x}^T = [x_1 \;\; x_2]$, $\mathbf{d}^T = [d_1 \;\; d_2]$ are the state and the input vectors, respectively, and $\tilde{d}_i = d_i - t_d/T$; $\mathbf{f}^T = \left[\frac{I_{b_1}}{\eta_1} \;\; \frac{I_{b_2}}{\eta_2}\right]$ is the function of cells' currents and $\mathbf{x}_{k_0}$ represent the initial SoC vector. The cost functions to be minimized are given as

$$J_1 = \sum_{k=K_0}^{k_0+H_P} \left[-w_x \left(\min(\mathbf{x})\right)^2 + \sum_{j=1}^{2} \left(I_{c_j}^2 + I_{d_j}^2 \right) \right], \tag{13}$$

$$\min(\mathbf{x}) = -\frac{1}{p} \log\left(\sum_{n=1}^{2} e^{-p x_n} \right),$$

$$J_2 = \sum_{k=K_0}^{k_0+H_P} \left[w_x \left(\max(\mathbf{x}) - \min(\mathbf{x})\right)^2 + \sum_{j=1}^{2} \left(I_{c_j}^2 + I_{d_j}^2 \right) \right], \tag{14}$$

$$\max(\mathbf{x}) = \frac{1}{p} \log\left(\sum_{n=1}^{2} e^{p x_n} \right),$$

$$J_3 = \sum_{k=K_0}^{k_0+H_P} \left[w_x \left(\sum_{n=1}^{2} (x_n - \bar{x})^2 \right) + \sum_{j=1}^{2} \left(I_{c_j}^2 + I_{d_j}^2 \right) \right], \tag{15}$$

$$\bar{x} = \frac{1}{2} \left(\sum_{n=1}^{2} x_n \right),$$

where $w_x = 20000$ represents the weight of first term in each cost function, $H_P = 10$ s is the prediction horizon and $p = 100$.

IV. Results and Discussion

To compare the performance of different cost functions, all physically aimed at achieving cell balancing but with different mathematical realizations, extensive simulations have been performed. In all the simulations, the battery is discharged to 10% of SoC, mimicking the shutdown scenario, and balancing time t_b is defined as a time instant (k) when the difference between cells's SoC becomes 0.02. It is pertinent to mention that cells' electrical dynamics are modeled using a first-order ECM model. In this scheme, the internal resistance $R0$ is dependent on SoC, and the map between SoC and OCV is approximated using polynomial fitting. Furthermore, the nominal model parameters used in the ACBN network are outlined in table I.

TABLE I: Nominal model parameters of ACBN

Parameter	Value	Parameter	Value
T	20 μs	t_d	2 μs
V_F	0.3 V	R_{ds}	5.3 mΩ
t_f	8 ns	t_{rr}	28 ns
R_L	0.01 Ω	L	0.3 μH

Figure 2 depicts the implementation of ACBN in closed-loop configuration. As SoC is not directly measurable, a state dependent Kalman filter (SDKF), which we designed in our earlier work [16], has been incorporated into this framework. SDKF takes in the values of $v_\mathbf{t}$ and $I_{bat}^{\mathbf{T}} = [I_{b_1} \quad I_{b_2}]$, quantities directly measurable, and based on these it gives an estimated value of SoC at each k; the values of SoC are then sent to NMPC block, which consequently generates duty cycles to perform the switching of the buck-boost converter. The nonlinear optimal control problem (NOCP) is solved in MATLAB through the CasADi toolbox, employing the interior point optimizer (Ipopt) algorithm. Moreover, to emulate the realistic scenarios, in ACBN, non-ideal values are set for resistances and capacities; similarly, a real-life driving profile US06 City, properly scaled down to fit in for 2 cells simulation— see Figure 4b, is considered as in input for ACBN. Expanding on the discussion, Figures 5, 6, and 7 depict the results of SoC, duty cycle, and balancing currents against cost functions J_1, J_2, and J_3 respectively. A cursory look of these results reveals a variation in NMPC performance in-terms of balancing time (t_b) and power losses ($\bar{P}_L$). J_1 has the fastest response in terms of balancing with 2745 s as the value of t_b, while also attaining the intermediary value of $\bar{P}_L$ at 342.56 mW. On the contrary, J_3 has the slowest response with 3815 s as t_b; however, it also succumbed to the lowest $\bar{P}_L$ of 335.57 mW. Finally, in terms of time, J_2 performance lies between the other two with a value of 3005 s; however, it also reported a maximum $\bar{P}_L$ of 350.37 mW. The visual quantification of this performance is also given in a bar graph, as depicted in Figure 3.

Due to the drive cycle current I_e, x_1 and x_2 decrease with time. The first term in each cost function dictates the value of t_b. In J_1, NMPC tries to maximize $\min(\mathbf{x})$ indefinitely, which keeps the first part of the cost function dominant throughout the simulation time, hence yielding minimum t_b. On the other hand $(\max(x) - \min(x))$, and $(x_i - \bar{x})$ reduce during cell balancing, hence giving more weight to the balancing currents, resulting in longer t_b as compared to J_1. Moreover, an inverse relationship exists between t_b and $\bar{P}_L$, emphasizing the need for trade-offs in selecting cost functions for NMPC formulation.

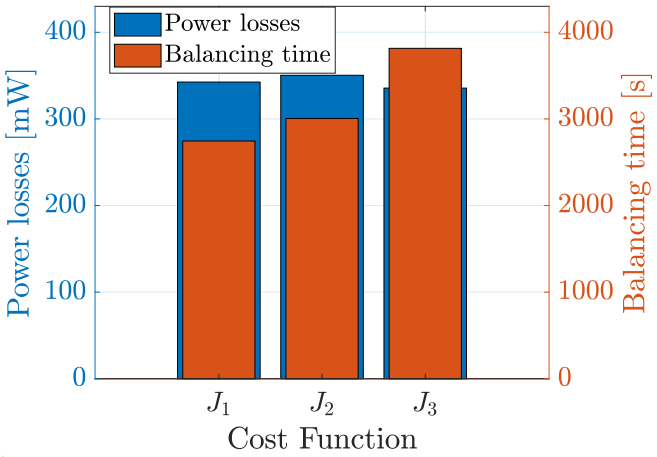

Fig. 3: Performance summary

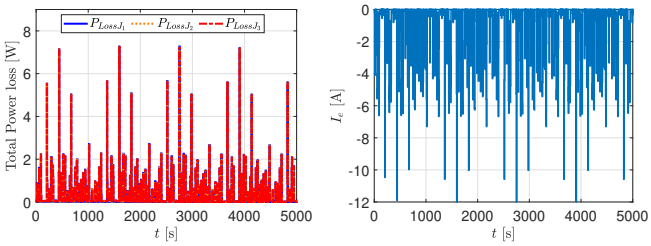

(a) Power Losses (b) US06 City current profile

Fig. 4: Power losses and drive cycle current with time.

V. Conclusion

To ensure optimal performance of a battery pack within an EV, a BMS module is integrated. Among other functions, it is tasked with ensuring that the SoC levels of all cells remain equal. In this context, MPC has received increased attention in contemporary research due to the versatility it offers. This leads to multiple design parameters in MPC synthesis, among which the design or selection of a cost function holds significant importance, resulting in varying closed-loop results. In this work, an NMPC problem is formulated aimed at active cell balancing within a battery pack. In this context, three different cost functions are considered, and a quantitative performance comparison in terms of t_b and $\bar{P}_L$ is conducted. The simulation results show that across different cost functions, while keeping all other parameters the same, a significant difference of 38.9% for t_b and 4.5% for $\bar{P}_L$ is observed.

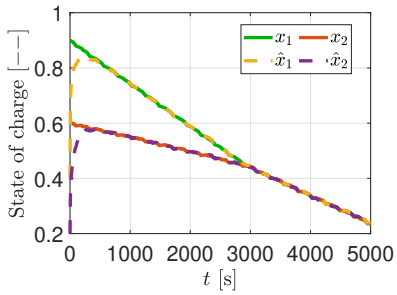

(a) True and estimated SoC

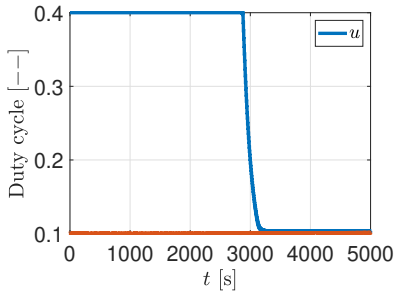

(b) Duty cycles

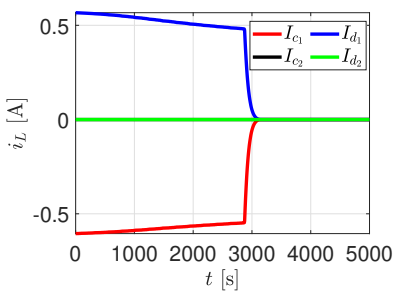

(c) Balancing currents

Fig. 5: Simulation results for J_1

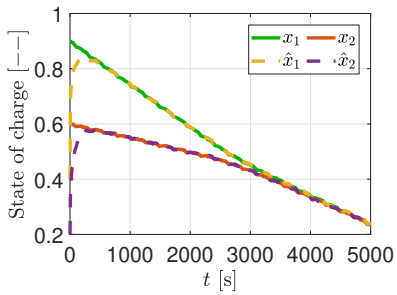

(a) True and estimated SoC

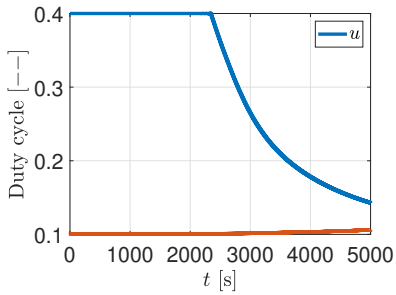

(b) Duty cycles

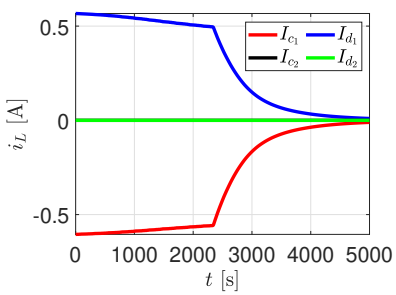

(c) Balancing currents

Fig. 6: Simulation results for J_2

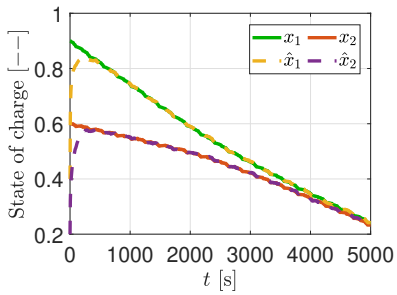

(a) True and estimated SoC

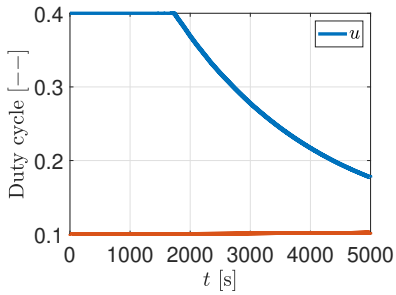

(b) Duty cycles

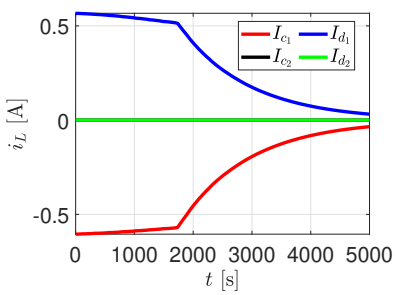

(c) Balancing currents

Fig. 7: Simulation results for J_3

A possible extension of this work is to integrate the thermal model into the battery pack and analyze the performance of various cost functions aimed at achieving thermal balancing in closed-loop setting.

References

[1] J. Liu, Y. Chen, and H. K. Fathy, "Nonlinear Model-Predictive Optimal Control of an Active Cell-to-Cell Lithium-Ion Battery Pack Balancing Circuit," *IFAC-PapersOnLine*, vol. 50, no. 1, pp. 14 483–14 488, Jul. 2017.

[2] F. S. J. Hoekstra, L. A. W. Ribelles, H. J. Bergveld, and M. C. F. Donkers, "Real-Time Range Maximisation of Electric Vehicles through Active Cell Balancing using Model-Predictive Control," in *2020 American Control Conference (ACC)*. IEEE, pp. 01–03.

[3] J. Chen, A. Behal, and C. Li, "Active Cell Balancing by Model Predictive Control for Real Time Range Extension," in *2021 60th IEEE Conference on Decision and Control (CDC)*. IEEE, pp. 14–17.

[4] C. N. Van and T. N. Vinh, "Optimal Cell Equalizing Control Based on State of Charge Feedback for Lithium-ion Battery Pack," *International Journal of Control, Automation and Systems*, vol. 21, no. 5, May 2023. [Online]. Available: https://doi.org/10.1007/s12555-021-0648-1

[5] C. N. Van, "Optimal Control of Active Cell Balancing for Lithium-Ion Battery Pack With Constraints on Cells' Current and Temperature," *Journal of Electrochemical Energy Conversion and Storage*, vol. 20, no. 1, p. 011009, 05 2022. [Online]. Available: https://doi.org/10.1115/1.4054530

[6] A. Heydarian and F. Abdollahi, "A Fast Balance Optimization Approach for Charging Enhancement of Lithium-Ion," Dec. 2023, [Online; accessed 1. Mar. 2024].

[7] J. Liu, Y. Chen, and H. K. Fathy, "Nonlinear model-predictive optimal control of an active cell-to-cell lithium-ion battery pack balancing circuit," *IFAC-PapersOnLine*, vol. 50, no. 1, pp. 14 483–14 488, 2017, 20th IFAC World Congress. [Online]. Available: https://www.sciencedirect.com/science/article/pii/S2405896317331087

[8] J. V. Barreras, C. Pinto, R. de Castro, E. Schaltz, S. J. Andreasen, and R. E. Araujo, "Multi-objective control of balancing systems for li-ion battery packs: A paradigm shift?" in *2014 IEEE Vehicle Power and Propulsion Conference (VPPC)*, 2014, pp. 1–7.

[9] J. V. Barreras, R. de Castro, Y. Wan, and T. Dragicevic, "A Consensus Algorithm for Multi-Objective Battery Balancing," *Energies*, vol. 14,

no. 14, p. 4279, Jul. 2021.
[10] J.-C. M. Lin, "Development of a globally active balance module with range extension effect," *IET Electr. Syst. Transp.*, vol. 7, no. 2, pp. 154–160, Jun. 2017.
[11] X. Lu and C. Wang, "Fuzzy Equalization Strategy Based on Multilayer Circuits," *JERR*, pp. 76–88, Jun. 2022.
[12] H. Wang, M. Rasheed, R. Hassan, M. Kamel, S. Tong, and R. Zane, "Life-Extended Active Battery Control for Energy Storage Using Electric Vehicle Retired Batteries," *IEEE Trans. Power Electron.*, vol. 38, no. 6, pp. 6801–6805, Mar. 2023.
[13] S. Singirikonda and Y. P. Obulesu, "Active cell voltage balancing of Electric vehicle batteries by using an optimized switched capacitor strategy," *J. Energy Storage*, vol. 38, p. 102521, Jun. 2021.
[14] A. Pozzi, M. Zambelli, A. Ferrara, and D. M. Raimondo, "Balancing-aware charging strategy for series-connected lithium-ion cells: A nonlinear model predictive control approach," *IEEE Transactions on Control Systems Technology*, vol. 28, no. 5, pp. 1862–1877, 2020.
[15] V. Azimi, A. Allam, and S. Onori, "Extending life of lithium-ion battery systems by embracing heterogeneities via an optimal control-based active balancing strategy," *IEEE Transactions on Control Systems Technology*, vol. 31, no. 3, pp. 1235–1249, 2023.
[16] A. A. Uppal, S. B. Javed, and Q. Ahmed, "Power Losses Aware Nonlinear Model Predictive Control Design for Active Cell Balancing," *IEEE Control Syst. Lett.*, vol. 7, pp. 3705–3710, Dec. 2023.